Search for the disappearance of muon antineutrinos in the NuMI neutrino beam

P. Adamson *et al.* (The MINOS Collaboration)

Phys. Rev. D **84**, 071103 — Published 11 October 2011

DOI: 10.1103/PhysRevD.84.071103

FERMILAB-PUB-11-357-PPD, BNL-96122-2011-JA, arXiv:hep-ex/1108.1509

Search for the disappearance of muon antineutrinos in the NuMI neutrino beam

P. Adamson,[7] D. J. Auty,[24] D. S. Ayres,[1] C. Backhouse,[18] G. Barr,[18] M. Bishai,[3] A. Blake,[5] G. J. Bock,[7] D. J. Boehnlein,[7] D. Bogert,[7] S. V. Cao,[26] S. Cavanaugh,[9] D. Cherdack,[27] S. Childress,[7] B. C. Choudhary,[7] J. A. B. Coelho,[6] S. J. Coleman,[29] L. Corwin,[12] D. Cronin-Hennessy,[15] I. Z. Danko,[19] J. K. de Jong,[18] N. E. Devenish,[24] M. V. Diwan,[3] M. Dorman,[14] C. O. Escobar,[6] J. J. Evans,[14] E. Falk,[24] G. J. Feldman,[9] M. V. Frohne,[10] H. R. Gallagher,[27] R. A. Gomes,[8] M. C. Goodman,[1] P. Gouffon,[21] N. Graf,[11] R. Gran,[16] N. Grant,[20] K. Grzelak,[28] A. Habig,[16] J. Hartnell,[24,20] R. Hatcher,[7] A. Himmel,[4] A. Holin,[14] C. Howcroft,[4] X. Huang,[1] J. Hylen,[7] G. M. Irwin,[23] Z. Isvan,[19] D. E. Jaffe,[3] C. James,[7] D. Jensen,[7] T. Kafka,[27] S. M. S. Kasahara,[15] G. Koizumi,[7] S. Kopp,[26] M. Kordosky,[29] A. Kreymer,[7] K. Lang,[26] G. Lefeuvre,[24] J. Ling,[3,22] P. J. Litchfield,[15,20] L. Loiacono,[26] P. Lucas,[7] W. A. Mann,[27] M. L. Marshak,[15] M. Mathis,[29] N. Mayer,[12] R. Mehdiyev,[26] J. R. Meier,[15] M. D. Messier,[12] D. G. Michael,[4,*] W. H. Miller,[15] S. R. Mishra,[22] J. Mitchell,[5] C. D. Moore,[7] L. Mualem,[4] S. Mufson,[12] J. Musser,[12] D. Naples,[19] J. K. Nelson,[29] H. B. Newman,[4] R. J. Nichol,[14] J. A. Nowak,[15] J. P. Ochoa-Ricoux,[4] W. P. Oliver,[27] M. Orchanian,[4] R. Pahlka,[7] J. Paley,[1,12] R. B. Patterson,[4] G. Pawloski,[23] G. F. Pearce,[20] S. Phan-Budd,[1] R. K. Plunkett,[7] X. Qiu,[23] J. Ratchford,[26] B. Rebel,[7] C. Rosenfeld,[22] H. A. Rubin,[11] M. C. Sanchez,[13,1,9] J. Schneps,[27] A. Schreckenberger,[15] P. Schreiner,[1] R. Sharma,[7] A. Sousa,[9] M. Strait,[15] N. Tagg,[17] R. L. Talaga,[1] M. A. Tavera,[24] J. Thomas,[14] M. A. Thomson,[5] G. Tinti,[18] R. Toner,[5] D. Torretta,[7] G. Tzanakos,[2] J. Urheim,[12] P. Vahle,[29] B. Viren,[3] J. J. Walding,[29] A. Weber,[18,20] R. C. Webb,[25] C. White,[11] L. Whitehead,[3] S. G. Wojcicki,[23] T. Yang,[23] and R. Zwaska[7]

(The MINOS Collaboration)

[1] *Argonne National Laboratory, Argonne, Illinois 60439, USA*
[2] *Department of Physics, University of Athens, GR-15771 Athens, Greece*
[3] *Brookhaven National Laboratory, Upton, New York 11973, USA*
[4] *Lauritsen Laboratory, California Institute of Technology, Pasadena, California 91125, USA*
[5] *Cavendish Laboratory, University of Cambridge, Madingley Road, Cambridge CB3 0HE, United Kingdom*
[6] *Universidade Estadual de Campinas, IFGW-UNICAMP, CP 6165, 13083-970, Campinas, SP, Brazil*
[7] *Fermi National Accelerator Laboratory, Batavia, Illinois 60510, USA*
[8] *Instituto de Física, Universidade Federal de Goiás, CP 131, 74001-970, Goiânia, GO, Brazil*
[9] *Department of Physics, Harvard University, Cambridge, Massachusetts 02138, USA*
[10] *Holy Cross College, Notre Dame, Indiana 46556, USA*
[11] *Department of Physics, Illinois Institute of Technology, Chicago, Illinois 60616, USA*
[12] *Indiana University, Bloomington, Indiana 47405, USA*
[13] *Department of Physics and Astronomy, Iowa State University, Ames, Iowa 50011 USA*
[14] *Department of Physics and Astronomy, University College London, Gower Street, London WC1E 6BT, United Kingdom*
[15] *University of Minnesota, Minneapolis, Minnesota 55455, USA*
[16] *Department of Physics, University of Minnesota – Duluth, Duluth, Minnesota 55812, USA*
[17] *Otterbein College, Westerville, Ohio 43081, USA*
[18] *Subdepartment of Particle Physics, University of Oxford, Oxford OX1 3RH, United Kingdom*
[19] *Department of Physics and Astronomy, University of Pittsburgh, Pittsburgh, Pennsylvania 15260, USA*
[20] *Rutherford Appleton Laboratory, Science and Technologies Facilities Council, OX11 0QX, United Kingdom*
[21] *Instituto de Física, Universidade de São Paulo, CP 66318, 05315-970, São Paulo, SP, Brazil*
[22] *Department of Physics and Astronomy, University of South Carolina, Columbia, South Carolina 29208, USA*
[23] *Department of Physics, Stanford University, Stanford, California 94305, USA*
[24] *Department of Physics and Astronomy, University of Sussex, Falmer, Brighton BN1 9QH, United Kingdom*
[25] *Physics Department, Texas A&M University, College Station, Texas 77843, USA*
[26] *Department of Physics, University of Texas at Austin, 1 University Station C1600, Austin, Texas 78712, USA*
[27] *Physics Department, Tufts University, Medford, Massachusetts 02155, USA*
[28] *Department of Physics, University of Warsaw, Hoża 69, PL-00-681 Warsaw, Poland*
[29] *Department of Physics, College of William & Mary, Williamsburg, Virginia 23187, USA*

We report constraints on antineutrino oscillation parameters that were obtained by using the two MINOS detectors to measure the 7% muon antineutrino component of the NuMI neutrino beam. In the Far Detector, we select 130 events in the charged-current muon antineutrino sample, compared to a prediction of $136.4 \pm 11.7(\text{stat})^{+10.2}_{-8.9}(\text{syst})$ events under the assumption $|\Delta\overline{m}^2| = 2.32 \times 10^{-3}$ eV^2, $\sin^2(2\overline{\theta}) = 1.0$. Assuming no oscillations occur at the Near Detector baseline, a fit to the two-flavor

oscillation approximation constrains $|\Delta\overline{m}^2| < 3.37 \times 10^{-3}\,\mathrm{eV}^2$ at the 90% confidence level with $\sin^2(2\overline{\theta}) = 1.0$.

PACS numbers: 14.60.Lm, 14.60.Pq, 29.27.-a, 29.30.-h

The phenomenon of neutrino oscillations has been well established by experimental observations [1–8]. The underlying quantum-mechanical mixing between the neutrino flavor and mass eigenstates is governed by the elements of the PMNS matrix [9], usually parameterized by three mixing angles and a CP-violating phase. Oscillations are governed by the ratio of the distance traveled by the neutrino to its energy (L/E) and the two independent neutrino mass-squared differences. CPT symmetry constrains the allowed differences between a particle and its antiparticle [10] and requires their masses to be identical. Differences between the measured neutrino and antineutrino oscillation parameters would indicate new physics. For example, as neutrinos propagate through matter, nonstandard interactions [11] could alter the disappearance probabilities of neutrinos relative to antineutrinos and thus the inferred oscillation parameters [12]. Such models of new physics predict a different energy dependence and so probing the standard oscillation hypothesis to greater precision across a wide range of energies is valuable.

The MINOS long-baseline experiment has made the most precise measurements to date of the larger (atmospheric) mass-squared splitting for both neutrinos [13] and antineutrinos [14]. With the NuMI facility [15] configured to provide a neutrino-dominated beam, a measurement of ν_μ disappearance resulted in a mass-squared splitting of $|\Delta m^2| = (2.32^{+0.12}_{-0.08}) \times 10^{-3}$ eV^2 and mixing angle $\sin^2(2\theta) > 0.90$ (90% confidence limit [C.L.]) [13, 16]. From direct observations of $\overline{\nu}_\mu$ disappearance, using a smaller exposure to the beam optimized for antineutrinos, MINOS measures the antineutrino oscillation parameters $|\Delta\overline{m}^2| = [3.36^{+0.46}_{-0.40}(\mathrm{stat}) \pm 0.06(\mathrm{syst})] \times 10^{-3}$ eV^2 and $\sin^2(2\overline{\theta}) = 0.86^{+0.11}_{-0.12}(\mathrm{stat}) \pm 0.01(\mathrm{syst})$ [14]. Prior to the measurement of $|\Delta\overline{m}^2|$ by MINOS the strongest constraints on antineutrino oscillation parameters came from a fit [17] to global data dominated by Super-Kamiokande results where the sum of atmospheric ν_μ and $\overline{\nu}_\mu$ interaction rates was measured.

This paper describes an analysis of the 7% $\overline{\nu}_\mu$ component of the NuMI beam, optimized to produce neutrinos, with an exposure of 7.1×10^{20} protons on target. The MINOS detectors are magnetized, allowing event-by-event separation of ν_μ and $\overline{\nu}_\mu$ charged-current (CC) events using the curvature of the muon track. The $\overline{\nu}_\mu$ sample presented here provides a new test of the oscillation hypothesis for muon antineutrinos at the atmospheric scale. With substantially increased statistics in the 5–15 GeV energy range relative to the sample obtained with the beam configured for antineutrinos [14] the $\overline{\nu}_\mu$ oscillation probability can be probed to greater precision in this region.

The NuMI beam uses 120 GeV/c protons incident on a graphite target to produce secondary hadrons, in particular pions and kaons of both charges. Depending on the sign of the applied current, two magnetic horns focus either positively or negatively charged hadrons for a neutrino or antineutrino beam, respectively. A 675 m long iron-walled decay pipe — evacuated during the first half of the data taking period but later filled with 0.9 atm helium for structural reasons — allows the hadrons and tertiary muons to decay in flight, producing neutrinos and antineutrinos. The antineutrino component of the neutrino beam arises from four main sources: decays of hadrons traveling along the axes of the horns where the focusing field is negligible; partially defocused hadrons decaying close to the horns; decays of hadrons produced from interactions with the helium and walls of the decay pipe; and decays of tertiary muons that arise mainly from decays of the focused hadrons. Muon antineutrinos from neutral kaons are estimated from simulation to comprise 0.6% of events across the spectrum. The combined energy spectrum of the $\overline{\nu}_\mu$ CC events arising from these sources is broadly distributed and peaks at approximately 8 GeV, whereas the energy spectrum resulting from the focused hadrons is narrowly-peaked at approximately 3 GeV.

The two MINOS detectors [18] are located 1.04 km [Near Detector (ND)] and 735 km [Far Detector (FD)] from the target. Both detectors are segmented steel/scintillator tracking calorimeters. The detector fiducial masses are 23.7 tons and 4.2 kilotons at the ND and FD respectively. In CC interactions, $\nu_\mu(\overline{\nu}_\mu) + \mathrm{N} \to \mu^-(\mu^+) + X$, a hadronic shower ($X$) and a muon track may be observed. The reconstructed neutrino energy is the sum of the reconstructed muon and hadron energies. Hadronic energy is measured by calorimetry. Muon energy is measured by range for contained tracks or by curvature in a 1.4 T toroidal magnetic field for exiting tracks. For this data set, the fields in both detectors have been set so that they focus μ^- and defocus μ^+, allowing the separation of ν_μ and $\overline{\nu}_\mu$ CC interactions.

The inclusive $\overline{\nu}_\mu$ CC interaction rate as a function of reconstructed $\overline{\nu}_\mu$ energy is measured in each detector. The measured FD spectrum is compared to the projection of the ND data to the FD, taking into account the different geometric acceptances of the two detectors. In this comparison, many sources of systematic uncertainty largely cancel due to the similarities of the two detectors. Antineutrino oscillations would cause an energy-dependent $\overline{\nu}_\mu$ deficit at the FD compared to the projection from the

*Deceased.

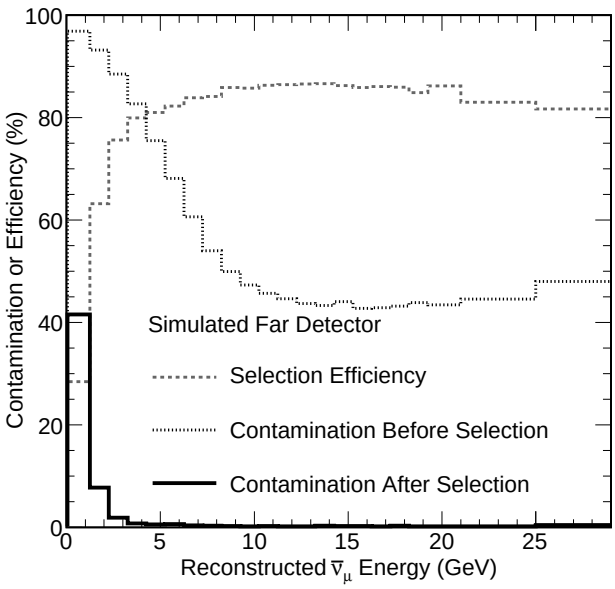

FIG. 1: Efficiency of the selection of $\bar{\nu}_\mu$ CC candidate events reconstructed with a positive charge-sign track in the Far Detector. The contamination due to misidentified NC and ν_μ CC interactions is also shown (assuming no oscillations), both before and after all other selection criteria are applied.

ND; the $\overline{\nu}_\mu$ survival probability in the two-flavor approximation is

$$P(\overline{\nu}_\mu \to \overline{\nu}_\mu) = 1 - \sin^2(2\overline{\theta}) \sin^2\left(\frac{1.267\Delta\overline{m}^2 L}{E}\right), \quad (1)$$

where L [km] is the distance from the point of antineutrino production, E [GeV] the antineutrino energy, $\overline{\theta}$ the antineutrino mixing angle, and $\Delta\overline{m}^2$ [eV^2] the antineutrino mass-squared difference.

Selected events must contain at least one reconstructed track; the longest track is identified as the muon candidate. This muon candidate must originate inside the fiducial volume and have a positive charge determined from track curvature. However, the track finding algorithm can occasionally form a track out of hadronic activity, or misidentify the curvature of a muon track. A simple charge-sign selection based on this track-fit information yields a sample that is highly contaminated with both ν_μ CC and neutral current (NC) events as shown in Fig. 1. Monte Carlo studies show that about half of NC events with a reconstructed track and 7% of ν_μ CC events with a track are misidentified as μ^+ candidates. Most of the misidentified ν_μ CC events are high-inelasticity interactions in which the soft μ^- is obscured by the hadronic shower. In addition, higher momentum muons follow a less curved trajectory, increasing the probability of charge misidentification. With the beam consisting of about 92% muon neutrinos, the initial signal to background ratio is inherently much lower for muon antineutrinos than it is for neutrinos and the development of further selection cuts was necessary.

To reduce the misidentified NC and ν_μ CC background events, three selection variables are used. The first is a likelihood-based separation parameter based on event topology. The second variable is a measure of the confidence of charge-sign determination from the track fitting. The third variable provides an additional measure of the direction of curvature of the muon track by comparing the local track direction at the vertex to that at the end point of the track [19]. The likelihood-based separation parameter was originally developed to distinguish NC background from ν_μ CC events in the MINOS analysis of ν_μ oscillations [1] but it is also effective in removing the misidentified high-inelasticity ν_μ CC background. This discriminator uses probability density functions constructed from three variables: the event length, the fraction of the total event signal in the reconstructed track, and the average signal per plane of the reconstructed track. These quantities are related to the muon range, the event inelasticity and the average energy loss $\mathrm{d}E/\mathrm{d}x$ of the muon track and are distributed differently for $\overline{\nu}_\mu$ CC events compared to NC and misidentified ν_μ CC events.

The selection was optimized [20] for statistical sensitivity to oscillation parameters equal to those measured for ν_μ [21]. Figure 1 shows the efficiency of the full selection and the remaining contamination as a function of $\overline{\nu}_\mu$ energy in the FD. Assuming no oscillations, the efficiency of the selection is 85% and the purity of the $\overline{\nu}_\mu$ CC sample is 98%, integrated over all energies in the FD.

The measured ND energy spectrum, shown in Fig. 2, is used to predict the FD spectrum, as in previous MINOS analyses [1, 13, 21, 22]. This effectively mitigates sources of mismodeling, such as uncertainties in the neutrino flux or neutrino cross sections, which affect both detectors in similar ways.

Hadron production in the NuMI target and beam line is simulated with FLUKA [23] by using FLUGG [24] as an interface to the GEANT4 [25] based geometry. Additionally, hadron production in the target is constrained by a fit to ND spectra [1], which correct the π and K distributions as a function of their transverse and longitudinal momenta at production, p_{T} and p_z respectively. The fit is performed simultaneously for several different beam configurations, which permits the constraint of a wide range of p_{T}-p_z space for ν_μ parent particles. The π^+/π^- ratio measured by NA49 [26], together with the p_{T} spectral shape from the ν_μ fit, constrains the $\overline{\nu}_\mu$ parent p_{T} spectral shape, while a fit to the ND $\overline{\nu}_\mu$ energy spectrum provides overall normalization and p_z shape information. These fit parameters have been applied to the flux in obtaining the simulated ND spectrum shown in Fig. 2. The errors obtained in the fit provide an estimate of the uncertainty on the hadron production from the target; the corresponding error on the FD event rate, extrapolated from ND data, is less than 1% for the beam component that arises directly from hadrons produced in the target.

Figure 2 shows the contribution of different beam flux components to the $\overline{\nu}_\mu$ CC interaction rate in the ND

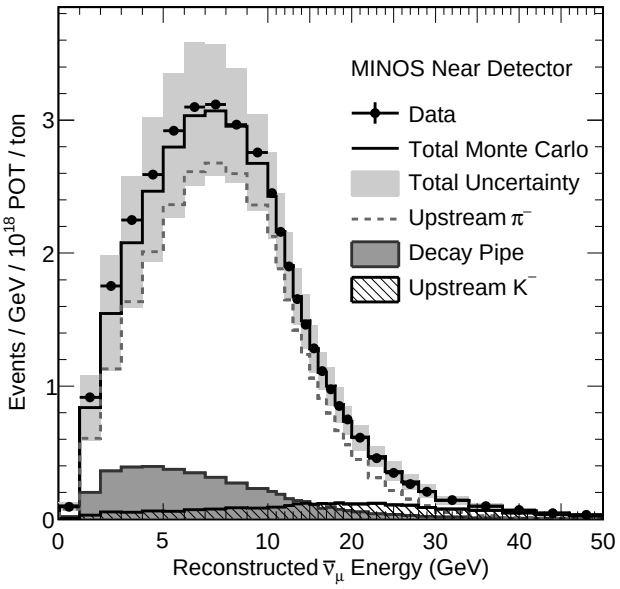

FIG. 2: Reconstructed energy spectra of $\overline{\nu}_\mu$ CC candidate events at the Near Detector. The solid line shows the Monte Carlo simulation, which is broken into three sources of $\overline{\nu}_\mu$ parent particles. The upstream pion decay contribution originates primarily from the target but also includes antineutrinos from muons whose parents decayed in the upstream region. The decay pipe component corresponds to all $\overline{\nu}_\mu$ parents (other than muons, which contribute about 3% of the ND spectrum) produced 45 m or more downstream of the target. The contribution from kaon decay is shown by the hatched histogram. The shaded band on the simulation shows the size of the systematic error on the absolute ND spectrum prediction.

as a function of energy. A significant fraction of ND events originate from parent particles produced in the decay pipe, predominantly from interactions of primary and secondary hadrons with the decay pipe walls and the helium (muons are not included in our decay pipe component definition as they are constrained by the ND ν_μ CC events). For these events the relative acceptance of the ND compared to the FD is larger than for particles produced in upstream interactions. Consequently, the contribution from decay pipe parent particles as a fraction of the total spectrum is larger at the ND (12%) compared to the FD (7%, assuming no oscillations). A systematic uncertainty on the size of the decay pipe component was assessed by scaling this component in the Monte Carlo simulation and comparing with the ND data. Conservative scale factors of ±100% are applied to the decay pipe component, introducing an uncertainty on the total $\overline{\nu}_\mu$ CC interaction rate predicted at the FD of $^{+6.2}_{-5.0}$%.

Further systematic uncertainties include a 4% relative normalization uncertainty between the ND and FD to account for uncertainties in the reconstruction efficiencies, exposure and fiducial masses of both detectors [21]. A comparison of momentum measurement from curvature vs. range in stopping muon tracks constrains the uncertainty in track momentum determination from curvature to be 4%. The 50% uncertainty on the misidentified NC and ν_μ CC events was estimated by scaling those components in the ND until the MC matched the data for the set of events that narrowly failed the selection on the likelihood-based separation parameter. The total systematic uncertainty on the predicted number of events at the FD is 82% of the total statistical uncertainty, assuming oscillation parameters equal to those measured for ν_μ [13].

Run period	POT (10^{20})	Events observed	Events expected (oscillated)	Events expected (no osc.)
I & II	3.21	43	$60.2^{+8.7}_{-8.5}$	$66.4^{+9.2}_{-9.0}$
III	3.88	87	$76.2^{+10.9}_{-10.2}$	$83.9^{+11.6}_{-10.9}$
Total	7.09	130	$136.4^{+15.5}_{-14.7}$	$150.3^{+16.6}_{-15.6}$

TABLE I: Candidate $\overline{\nu}_\mu$ CC events observed and expected in the Far Detector, broken down into two periods of approximately equal exposure. The expected number of events in the oscillated case uses the parameters measured with the ν_μ CC sample [13].

At the FD a total of 130 selected $\overline{\nu}_\mu$ CC candidate events are observed. Figure 3 shows the energy spectrum of the FD data overlaid with two predicted spectra obtained from the ND data: one without oscillations and one with oscillation parameters of $|\Delta\overline{m}^2| = 2.32 \times 10^{-3}$ eV^2, $\sin^2(2\overline{\theta}) = 1.0$ [13]. The predicted backgrounds are 1.8 ν_μ CC events, 1.2 NC events and 0.2 $\overline{\nu}_\tau$ CC events (in the oscillated case). The integrated number of events observed and expected are detailed in Table I. The number of FD events measured in run periods I and II is smaller than the prediction. In run period III, which differs due to the helium in the decay pipe, a larger number of events are measured compared with the prediction. The probability of observing a comparable or larger difference in event rate between the two periods, evaluated using mock Monte Carlo experiments, is 8.4%.

The measured FD energy spectrum is compared to that predicted from the ND assuming $\overline{\nu}_\mu \to \overline{\nu}_\tau$ oscillations, following Eq. (1). This comparison is made by minimizing a binned log-likelihood with respect to $\Delta\overline{m}^2$ and $\sin^2(2\overline{\theta})$. The Feldman-Cousins approach [27] is used to obtain confidence limits on the oscillation parameters with systematic uncertainties included [28, 29]. The confidence limits thus obtained are shown in Fig. 4. Values of $|\Delta\overline{m}^2|$ greater than 1 eV^2 are not considered in this analysis, since above that point oscillations with maximal mixing would cause more than 1% of the $\overline{\nu}_\mu$ to disappear in the ND. Figure 4 also shows the recent MINOS result using the beam configured for antineutrinos [14], the MINOS allowed region for neutrinos [13], and a fit [17] to all global data available prior to all MINOS $\overline{\nu}_\mu$ data. The MINOS data presented in this paper

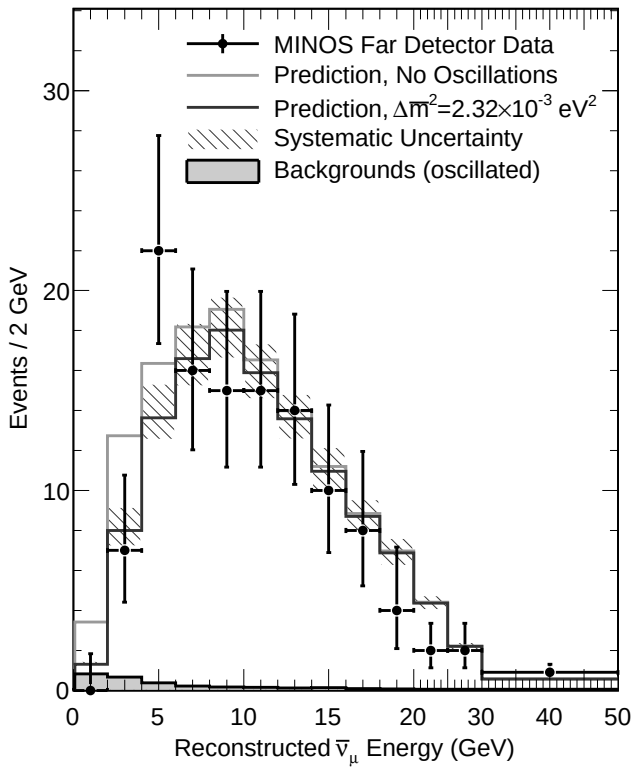

FIG. 3: Energy spectra of $\overline{\nu}_\mu$ CC candidate events observed in the Far Detector. The predicted spectrum with no oscillations and with oscillation parameter values of $|\Delta\overline{m}^2| = |\Delta m^2| = 2.32 \times 10^{-3}\,\mathrm{eV}^2$, $\sin^2(2\overline{\theta}) = \sin^2(2\theta) = 1.0$ are overlaid. The hatched band indicates the total systematic uncertainty on the prediction. The estimated background includes oscillations at the best-fit values determined by the MINOS ν_μ CC disappearance analysis [13] for the ν_μ CC events.

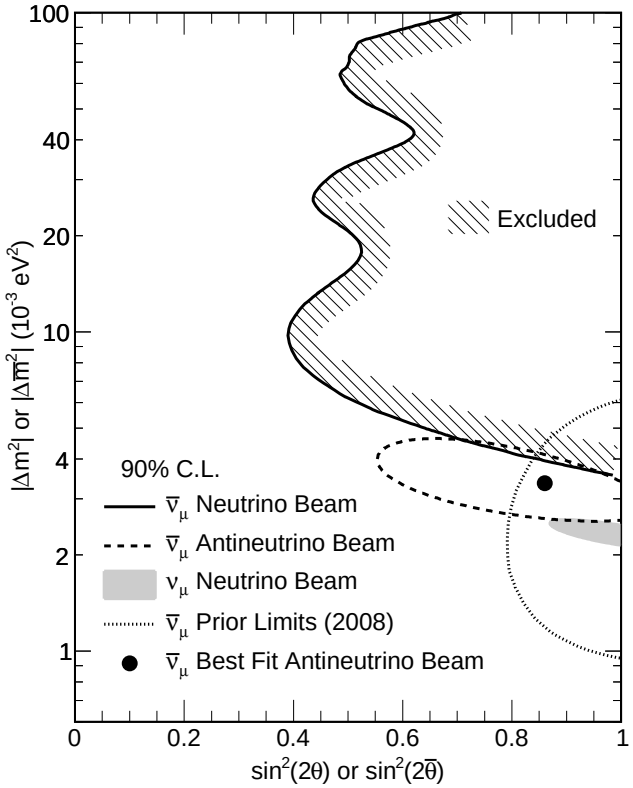

FIG. 4: Allowed regions for $\overline{\nu}_\mu$ oscillation parameters from a fit to the data in Fig. 3. The region indicated by the hashing is excluded. Shown alongside are contours for: the MINOS $\overline{\nu}_\mu$ result from the NuMI beam optimized for antineutrino production [14]; the MINOS allowed region for neutrinos [13]; and limits from a fit [17] prior to all MINOS $\overline{\nu}_\mu$ data.

are consistent with both the previous MINOS neutrino and antineutrino limits, and with the limits from a global fit [17]. A χ^2 goodness-of-fit test using the oscillation parameters from [13] yields a probability of 18%. Under the assumption $\sin^2(2\overline{\theta}) = 1.0$ these data constrain $|\Delta\overline{m}^2| < 3.37 \times 10^{-3}\,\mathrm{eV}^2$ (90% C.L.) in the two-flavor approximation.

In summary, a high-purity sample of muon antineutrino charged-current events was selected in the MINOS data from the 7% $\overline{\nu}_\mu$ component of the NuMI neutrino beam. At the Far Detector, 130 $\overline{\nu}_\mu$ event candidates were observed, which is consistent with the predicted rate in the case of oscillations of $136.4 \pm 11.7(\text{stat})^{+10.2}_{-8.9}(\text{syst})$ under the assumption $|\Delta\overline{m}^2| = 2.32 \times 10^{-3}$ eV^2, $\sin^2(2\overline{\theta}) = 1.0$. These data provide a new probe of the oscillation hypothesis for muon antineutrinos at the atmospheric scale. Significantly increased statistics in the 5–15 GeV energy range, compared to the $\overline{\nu}_\mu$ sample obtained with the NuMI beam configured for antineutrinos, have allowed the oscillation probability to be measured with greater precision in this region and have added to constraints on antineutrino oscillation parameters.

This work was supported by the U.S. DOE; the United Kingdom STFC; the U.S. NSF; the State and University of Minnesota; the University of Athens, Greece; and Brazil's FAPESP and CNPq. We are grateful to the Minnesota Department of Natural Resources, the crew of the Soudan Underground Laboratory, and the personnel of Fermilab for their contribution to this effort.

[1] D. G. Michael *et al.* (MINOS), Phys. Rev. Lett. **97**, 191801 (2006); P. Adamson *et al.* (MINOS), Phys. Rev. D **77**, 072002 (2008).
[2] Y. Ashie *et al.* (Super-Kamiokande), Phys. Rev. Lett. **93**, 101801 (2004); Phys. Rev. D **71**, 112005 (2005).
[3] B. Aharmin *et al.* (SNO), Phys. Rev. C **72**, 055502 (2005).
[4] T. Araki *et al.* (KamLAND), Phys. Rev. Lett. **94**, 081801 (2005).
[5] C. Arpesella *et al.* (Borexino), Phys. Rev. Lett. **101**, 091302 (2008).
[6] W. W. M. Allison *et al.* (Soudan-2), Phys. Rev. D **72**, 052005 (2005).
[7] M. Ambrosio *et al.* (MACRO), Eur. Phys. J. C **36**, 323 (2004).
[8] M. H. Ahn *et al.* (K2K), Phys. Rev. D **74**, 072003 (2006).
[9] B. Pontecorvo, JETP **34**, 172 (1958); V. N. Gribov and B. Pontecorvo, Phys. Lett. B **28**, 493 (1969); Z. Maki, M. Nakagawa, and S. Sakata, Prog. Theor. Phys. **28**, 870 (1962).
[10] See, for example, S. Weinberg, *The Quantum Theory of Fields* (Cambridge University Press, Cambridge, England, 1995), Vol. I.
[11] L. Wolfenstein, Phys. Rev. D **17**, 2369 (1978); J. W. F. Valle, Phys. Lett. B **199**, 432 (1987); M. C. Gonzalez-Garcia *et al.*, Phys. Rev. Lett. **82**, 3202 (1999); A. Friedland, C. Lunardini, and M. Maltoni, Phys. Rev. D **70**, 111301 (2004).
[12] Recent papers have discussed the compatibility of such nonstandard interactions with MINOS data: W. A. Mann *et al.*, Phys. Rev. D **82**, 113010 (2010); J. Kopp, P. A. N. Machado, and S. J. Parke, Phys. Rev. D **82**, 113002 (2010).
[13] P. Adamson *et al.* (MINOS), Phys. Rev. Lett. **106**, 181801 (2011).
[14] P. Adamson *et al.* (MINOS), Phys. Rev. Lett. **107**, 021801 (2011).
[15] K. Anderson *et al.*, FERMILAB-DESIGN-1998-01 (1998).
[16] The experiment measures an unresolved mixture of $|\Delta m^2_{31}|$ and $|\Delta m^2_{32}|$, which is referred to as $|\Delta m^2|$ for brevity. The parameter $\sin^2(2\theta)$ is likewise an admixture, dominated by θ_{23}. Similarly for $|\Delta\overline{m}^2|$ and $\sin^2(2\overline{\theta})$.
[17] M. C. Gonzalez-Garcia and M. Maltoni, Phys. Rept. **460**, 1 (2008). The contour shown in figure 4 was received through private communication.
[18] D. G. Michael *et al.* (MINOS), Nucl. Instrum. and Meth. A **596**, 190 (2008).
[19] R. Ospanov, Ph.D. thesis, University of Texas at Austin, 2008.
[20] D. J. Auty, D.Phil. thesis, University of Sussex, 2010.
[21] P. Adamson *et al.* (MINOS), Phys. Rev. Lett. **101**, 131802 (2008).
[22] J. J. Evans, D.Phil. thesis, University of Oxford, 2008.
[23] A. Ferrari, P. R. Sala, A. Fasso, and J. Ranft (2005), CERN-2005-10.
[24] G. Battistoni *et al.*, AIP Conf. Proc. **896**, 31 (2007).
[25] S. Agostinelli *et al.*, Nucl. Instrum. and Meth. A **506**, 250 (2003).
[26] C. Alt *et al.* (NA49), Eur. Phys. J. C **49**, 897 (2007).
[27] G. J. Feldman and R. D. Cousins, Phys. Rev. D **57**, 3873 (1998).
[28] N. E. Devenish, D.Phil. thesis, University of Sussex, 2011.
[29] A. I. Himmel, Ph.D. thesis, Caltech, 2011.